Polyhedron 225 (2022) 116045

Contents lists available at ScienceDirect

Polyhedron

journal homepage: www.elsevier.com/locate/poly

Analysis of spin frustration in an Fe^{III}_7 cluster using a combination of computational, experimental, and magnetostructural correlation methods

Ashlyn R. Hale [a,1], Lucas E. Aebersold [b], Juan E. Peralta [b,2], Dolos Foguet-Albiol [a], Khalil A. Abboud [a], George Christou [a,*,3]

[a] Department of Chemistry, University of Florida, Gainesville, FL 32611-7200, USA
[b] Department of Physics and Science of Advanced Materials, Central Michigan University, Mount Pleasant, MI 48859, USA

ARTICLE INFO

Keywords:
Cluster
Iron
Crystal structure
Magnetism
DFT

ABSTRACT

The synthesis, structure, and magnetic properties are reported for $[Fe_7O_3(O_2C^tBu)_9(mda)_3(H_2O)_3]$ (**1**), where $mdaH_2$ is *N*-methyldiethanolamine. **1** was prepared from the reaction of $[Fe_3O(O_2C^tBu)_6(H_2O)_3](NO_3)$ with $mdaH_2$ in a 1:~3 ratio in MeCN. The core of **1** consists of a central octahedral Fe^{III} ion held within a non-planar Fe_6 loop by three μ_3-O^{2-} and three μ_2-RO^- arms from the three mda^{2-} chelates. Variable-temperature dc and ac magnetic susceptibility studies revealed dominant antiferromagnetic coupling, leading to a ground state spin of $S = {}^5/_2$. The ground state was confirmed by a fit of magnetization data collected in the 0.1–7.0 T and 1.8–10.0 K ranges. The four Fe_2 pairwise exchange parameters (J_1-J_4) were estimated by independent methods: theoretical calculations using either broken symmetry energy differences (−46.3, −16.2, −3.9, and − 28.1 cm^{-1}, respectively) or Green's function approximation methods (−41.4, −14.8, −13.2, and − 24.7 cm^{-1}), and a magnetostructural correlation (MSC) previously developed for high nuclearity Fe^{III}/O complexes (−39.5, −13.8, −6.7, and − 23.5 cm^{-1}). Additionally, the J_1-J_4 obtained from the MSC and theoretical methods were used with the program PHI to both simulate $\chi_M T$ vs T as well as to serve as reasonable input values to fit the experimental data (−41.0, −11.4, −5.0, and − 27.3 cm^{-1}). Analysis of the J_{ij} led to identification of the spin frustration effects operative and the resultant spin vector alignments at each Fe^{III} ion, thus allowing for the rationalization of the experimental ground state.

1. Introduction

Fe^{III}/oxo chemistry lies at the intersection of diverse areas such as bioinorganic chemistry and molecular magnetism, giving rise to a rich library of Fe^{III}/oxo complexes ranging from synthetic mimics of diiron biomolecules, such as ribonucleotide reductase [1,2], hemerythrin [3], the soluble methane monooxygenase [2,4], and others [5], to high nuclearity complexes that could provide insight into the formation of potential nanoscale Fe^{III}/O/OH intermediates during the loading of the ferritin protein [6]. The formation of polynuclear Fe^{III}/oxo clusters results from the controlled hydrolysis of Fe^{III}, as the high charge-to-size ratio and Lewis acidity of Fe^{III} favour the formation of O^{2-} bridges via deprotonation of H_2O in situ. As oxo-bridged high-spin Fe^{III} ($S = {}^5/_2$) pairs almost always exhibit antiferromagnetic (**AF**) exchange couplings, high nuclearity Fe^{III}/oxo complexes provide many opportunities to analyze molecular spin frustration, i.e., competing exchange interactions, J_{ij}, of comparable magnitude that hinder or frustrate the preferred spin alignments [7]. Large ground state spins, S, often result from such spin frustration, providing the opportunity for the discovery of new Fe^{III} SMMs despite the lack of substantial magnetic anisotropy typically present in Fe^{III} clusters [8].

As the magnetic properties of Fe^{III}/oxo clusters are important for various applications, it is crucial to quantitatively understand the nature of the pairwise Fe_2 magnetic exchange interactions, J_{ij}, to enable rationalization and/or prediction of ground state spin values. Such a quantitative assessment of J_{ij} can also lead to identification of structural features that favor spin frustration and yield large ground state spins, S. Although multiple magnetostructural correlations (MSCs) for dinuclear

* Corresponding author.
E-mail address: christou@chem.ufl.edu (G. Christou).
[1] 0000-0001-5120-4693
[2] 0000-0003-2849-8472
[3] 0000-0001-5923-5523.

https://doi.org/10.1016/j.poly.2022.116045
Received 6 June 2022; Accepted 12 July 2022
Available online 16 July 2022

Table 1
Crystallographic information and structure refinement data for **1**.

Formula	$C_{60}H_{114}Fe_7N_3O_{30}$
FW (g/mol)	1748.49
Space group	*R*3
a (Å)	26.5134(8)
b (Å)	26.5134(8)
c (Å)	10.5013(6)
β ()	90
γ()	120
V (Å^3)	6393.0(5)
Z	3
T (K)	173(2)
λ (Å)	0.71073
ρ_{calc} (g/cm^3)	1.362
R_1 [a,b]	0.0388
wR_2 [a,c]	0.0792

$w = 1/[\sigma^2(Fo^2)+(m*p)^2 + n*p]$, $p = [\max(Fo^2, 0) + 2*Fc^2]/3$, m and n are constants.
[a] $I > 2\sigma(I)$.
[b] $R_1 = \Sigma(||F_o| - |F_c||) / \Sigma|F_o|$.
[c] $wR_2 = [\Sigma[w(F_o^2 - F_c^2)^2] / \Sigma[w(F_o^2)^2]]^{1/2}$.

Fe^{III}/oxo compounds have been developed over the years, we have found them poorly applicable to higher nuclearity Fe^{III}/oxo complexes [7,9]. The various J_{ij} in high nuclearity Fe^{III}/oxo complexes are also particularly difficult to determine from experimental or computational methods, owing to: (1) the many inequivalent J_{ij} typically present as nuclearity increases; (2) the lack of a reliable MSC for high nuclearity Fe^{III}/oxo clusters; (3) the increasing computational demands of theoretical methods as nuclearity increases; and (4) overparameterization and resulting false fits when fitting data with available fitting software. To address these issues, we developed the Mitchell-Christou (M−C) semiempirical MSC for polynuclear Fe^{III}/oxo complexes [9] based on the angular overlap model, finally providing a convenient route to reliable J_{ij} from the Fe-O bond lengths and Fe-O-Fe angles within each Fe_2 pair of a polynuclear cluster. This has allowed, among other things, rationalization of experimental ground state *S* values and reliable inputs for simulating and fitting the experimental data [9]. The development of the M−C polynuclear Fe^{III}/oxo MSC combined with the continually improving power of computational methods makes polynuclear Fe^{III}/oxo complexes enticing opportunities to analyze magnetic exchange couplings in greater detail than the status quo of the past.

In search of new polynuclear Fe^{III}/oxo complexes, a prolific synthetic strategy from our group and others is preparation of complexes containing both carboxylate and polyalkoxide chelating/bridging ligands, which has afforded an array of molecular architectures. For example, we previously reported an EPR spectral study of a new heptanuclear Fe^{III}/oxo complex, $[Fe_7O_3(O_2C^tBu)_9(mda)_3(H_2O)_3]$ (**1**) [10], discovered from such a reaction using *N*-methyldiethanolamine ($mdaH_2$) as the polyalcohol reagent. However, we never published the full synthetic, structural, and magnetic details as we could not obtain a suitably-refined publishable X-ray crystal structure at that time.

In the present work, we have optimized the synthesis of **1**, determined its crystal structure to a publishable level, and carried out a SQUID magnetometry study. Since **1** is an attractive candidate to test independent approaches to evaluating magnetic exchange couplings (J_{ij}), we have carried out a three-pronged experimental, computational, and magnetostructural correlation study, comprising (i) a detailed analysis of the exchange-coupling (J_{ij}) parameters from use of the M−C polynuclear MSC and theoretical calculations, (b) a comparison of two different theoretical methods for evaluating J_{ij}, standard broken symmetry energy differences and the Green's function approximation, (c) fitting using program PHI [11] of experimental $\chi_M T$ vs *T* data to obtain J_{ij}, and (d) rationalization of both the spin frustration effects operative and the resulting experimentally determined ground state spin.

2. Experimental

2.1. Synthesis

All manipulations were performed under aerobic conditions using chemicals as received from Fisher Scientific. $[Fe_3O(O_2C^tBu)_6(H_2O)_3](NO_3)$ was prepared as described elsewhere [12].

2.1.1. $[Fe_7O_3(O_2C^tBu)_9(mda)_3(H_2O)_3]$ (1)

To a stirred orange solution of $[Fe_3O(O_2C^tBu)_6(H_2O)_3](NO_3)$ (0.50 g, 0.55 mmol) in MeCN (25 mL) was added $mdaH_2$, (0.21 g, 1.8 mmol), causing a color change to brown. The solution was stirred for a further 4 h, filtered, and the filtrate carefully layered with an equal volume of Et_2O. Brown plate crystals of **1** slowly grew over a few days and were either maintained in the mother liquor for single-crystal X-ray crystallography, or collected by filtration, washed with MeCN, and dried in vacuo for other studies. The yield was 0.11 g (28 % based on Fe). Vacuum-dried material analyzed as solvent free. Anal. Calc (Found) for $C_{60}H_{120}Fe_7N_3O_{30}$: C 41.08 (41.27); H 6.90 (7.11); N, 2.40 (2.27). Selected IR data (KBr disk, cm^{-1}): 3522 (b,m), 2972 (m,sh), 2901 (m, sh), 2867 (m, sh), 2809 (w, sh), 2361 (w, sh), 2336 (w, sh), 1606 (s, sh), 1575 (s, sh), 1521 (w, sh), 1483 (s, sh), 1457 (w, sh), 1424 (s), 1363 (m, sh), 1262 (w, sh), 1228 (m, sh), 1098 (m, sh), 1058 (m), 1029 (m, sh), 1000 (m, sh), 904 (w, sh), 880 (w, sh), 789 (w, sh), 761 (w, sh), 679 (m, sh), 602 (m, sh), 581 (m, sh), 528 (m, sh), 484 (w), 438 (w, sh), 419 (w).

2.2. X-ray crystallography

Data were collected at 173 K on a Siemens SMART PLATFORM equipped with A CCD area detector and a graphite monochromator utilizing MoK_α radiation (λ = 0.71073 Å). Cell parameters were refined using 8192 reflections. A full sphere of data (1850 frames) was collected using the ω-scan method (0.3° framewidth). The first 50 frames were re-measured at the end of data collection to monitor instrument and crystal stability (maximum correction on *I* was <1 %). Absorption corrections by integration were applied based on measured indexed crystal faces. The structure was solved by direct methods and refined in *SHELXL* [13] using full-matrix least squares refinement on F^2. The non-H atoms were refined with anisotropic displacement parameters, and all H atoms were placed in calculated idealized positions and refined as riding on their parent atoms. R_1 is calculated to provide a reference to the conventional *R* value but its function is not minimized.

The asymmetric unit consists of $^1/_3$ of the Fe_7 cluster located on a 3-fold rotation axis. The H atoms (H8) on the coordinated H_2O molecule could not be found in a difference Fourier map and were thus calculated in idealized positions from the O8-H8···O9 hydrogen-bonding involving the H_2O ligand (O8) and an adjacent pivalate O atom, O9, resulting in twofold disorder of the second H (H8X/H8Y) of the H_2O ligands. Initial attempts to solve the structure in space group *R*3 did not refine well, as the wR_2 and R_1 remained at values over 50 % and 23 %, respectively. However, the structure refined very well and to low *R* values once the data were treated as a merohedral twin by switching the *a* and *b* axes and changing the sign of the *c* axis. In the final cycle of refinement, 6396 reflections (of which 5629 are observed with $I > 2\sigma$ (*I*)) were used to refine 302 parameters, and the resulting R_1, wR_2 and *S* (goodness of fit) were 3.88 %, 7.92 %, and 0.978, respectively. Crystal data and structure refinement parameters are listed in Table 1.

2.3. Physical measurements

Infrared spectra were recorded on crushed polycrystalline samples as KBr pellets on a Nicolet Nexus 670 FTIR spectrometer in the 400–4000 cm^{-1} range. Elemental analyses (C, H and N) were performed by Atlantic Microlab in Norcross, Georgia, USA. Variable-temperature dc and ac magnetic susceptibility data were collected using a Quantum Design MPMS-XL SQUID magnetometer equipped with a 7 Tesla magnet and

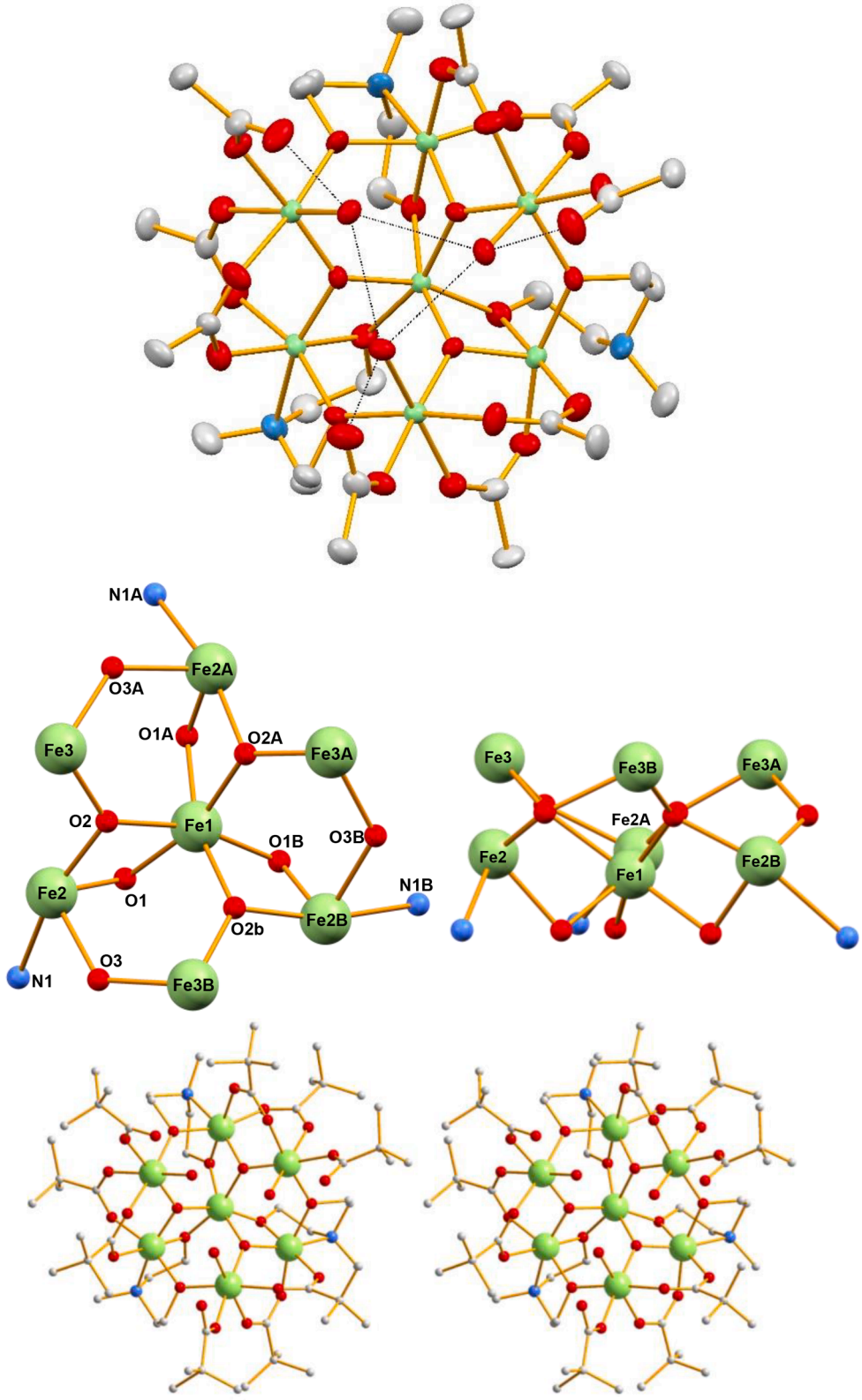

Fig. 1. (**top**) Complete structure of **1** with ^{t}Bu groups omitted for clarity; (**middle**) Top-view (left) and side-view (right) of the labelled Fe^{III}/O/N core; and (**bottom**) stereopair of the complete structure with H atoms are omitted for clarity. Color code: Fe^{III} lime green, O red, N powder blue, C grey. ((Colour online.))

operating in the 1.8–300 K range. Samples were embedded in solid eicosane to prevent torquing. Magnetization vs field and temperature data were fit using the program MAGNET [14], and D vs g fit error surfaces were generated using the program GRID [15]. Pascal's constants were used to estimate the diamagnetic correction [16], and contributions from the eicosane and gel capsule were measured as a blank. All these were subtracted from the experimental susceptibility to give the molar paramagnetic susceptibility (χ_M). Ac magnetic susceptibility measurements were carried out on a microcrystalline vacuum-dried sample in the 1.8 – 15.0 K range using a 3.5 G ac field and a 1000 Hz oscillation frequency.

Table 2
Selected interatomic distances (Å) and angles (°) for **1.**

Fe1-O1A	1.990(5)	Fe2-N1	2.232(7)
Fe1-O2A	2.024(5)	Fe3-O2	1.863(5)
Fe2-O2	1.883(5)	Fe3-O3B	1.989(6)
Fe2-O1	1.977(5)	Fe3-O7	2.032(5)
Fe2-O3	2.007(5)	Fe3-O10	2.034(6)
Fe2-O5	2.027(6)	Fe3-O8	2.072(5)
Fe2-O4	2.048(6)	Fe3-O6	2.073(6)
Fe2-O1-Fe1	96.9(2)	Fe3-O2-Fe2	119.8(3)
Fe3-O2-Fe1	134.6(3)	Fe2-O2-Fe1	98.9(2)
Fe3A-O3-Fe2	127.9(3)		

Table 3
Bond valence sums (BVS) and assignments [a] for the Fe and O atoms in **1.**

Atom	**Fe^{II}**	**Fe^{III}**
Fe1	2.64	**3.15**
Fe2	2.61	**3.10**
Fe3	2.63	**3.14**
Atom	**BVS**	**Assignment**
O2	2.00	O^{2-}
O8	0.42	H_2O
O4	1.87	$^tBuCO_2^-$
O5	1.80	$^tBuCO_2^-$
O6	2.01	$^tBuCO_2^-$
O7	1.87	$^tBuCO_2^-$
O9	1.55	$^tBuCO_2^-$
O10	1.78	$^tBuCO_2^-$
O1	2.01	mda^{2-}
O3	1.96	mda^{2-}

[a] The Fe oxidation state is the nearest integer to the bold value, which is the closest to the charge for which it was calculated. For O, values in the ~ 1.8–2.0, ~1.0–1.2, and ~ 0.2–0.4 ranges indicate non, single- and double-protonation, respectively, but can be affected by hydrogen-bonding.

2.4. Theoretical calculations

All magnetic exchange DFT calculations for the Fe_7 complex were performed using the X-ray structural data obtained in this work. These couplings were determined from DFT calculations by mapping broken-symmetry solutions to Ising-type spin configurations $\{S\}$ using the high-spin, all single-spin inversions, and all first-neighbor two-spin inversions. The energies of these configurations are expressed in terms of a sum over single-center interactions, Eq. (1), where $\langle ij \rangle$ means all ij pairs, $S_k = \pm^5/_2$ for Fe^{III}, and E_0 is a constant introduced to match the spin model with the DFT energies.

$$E(\{S\}) = -2\sum_{\langle ij \rangle} J_{ij} S_i \cdot S_j + E_0 \quad (1)$$

It should be noted that this approach reduces to the broken-symmetry formulation of Noodleman [17] for the case of two centers, Eq. (2),

$$J_{\Delta E} = \frac{E_{BS} - E_{HS}}{4 S_A S_B} \quad (2)$$

where E_{BS} and E_{HS} are the energies of the broken symmetry (BS) and high spin (HS) solutions, and S_A and S_B are the ideal spin quantum numbers for each center. To determine the exchange couplings J_{ij}, the energies of all spin configurations $\{S\}$ from broken spin-symmetry DFT calculations were employed to perform a linear regression fit of the Ising-type energy formula in Eq. (1). This approach has been successfully used in the past to determine magnetic exchange couplings in multi-center transition metal complexes [18]. The linear regression R^2 parameter differs from 1 by less than 10^{-6}, which shows that the magnetization is localized at the magnetic centers, and thus the broken-symmetry DFT solutions are reliably represented by the Ising-type model configurations. We have also verified that the atomic spin populations from the DFT calculations are consistent with the expected broken symmetry spin configuration.

The Green's function (GF) approach is another method to extract the exchange couplings from DFT calculations, initially developed by Liechtenstein [19] for the solid state. The GF approach has been formulated for its use in molecular complexes [20,21] by Steenbock et al. and adopted in this work. The GF approach, in brief, relies on an approximate expression that relates magnetic exchange couplings with differential local spin rotations [22]. The equation resulting from that

Table 4
Fe_7 clusters[a] containing a central Fe within an Fe_6 loop, and their cores and ground state spin.

Formula[a]	Core	Central Fe	S	Ref.
$[Fe_7O_3(O_2C^tBu)_9(mda)_3(H_2O)_3]$ [b]	$[Fe^{III}_7O_3]^{15+}$	oct Fe^{III}	$^5/_2$	t.w.
$[Fe_7O_3(O_2CPh)_9(mda)_3(H_2O)]$ [b]	$[Fe^{III}_7O_3]^{15+}$	oct Fe^{III}	$^5/_2$	27
$[Fe_7O_3(O_2C^tBu)_9(bda)_3(H_2O)_3]$ [b]	$[Fe^{III}_7O_3]^{15+}$	oct Fe^{III}	$^5/_2$	28
$[Fe_7O_3(O_2C^tBu)_9(phda)_3(H_2O)_3]$ [b]	$[Fe^{III}_7O_3]^{15+}$	oct Fe^{III}	$^5/_2$	28
$[Fe_7O_3(O_2C^tBu)_9(teaH)_3(H_2O)_3]$ [b]	$[Fe^{III}_7O_3]^{15+}$	oct Fe^{III}	$^5/_2$	28,29
$[Fe_7O_3(O_2C^tBu)_9(bheapH)_3(H_2O)_3]$ [b]	$[Fe^{III}_7O_3]^{15+}$	oct Fe^{III}	$^5/_2$	29
$[Fe_7O_3(OH)_3(hmpip)_6(O_2CPh)_7]^-$ [c]	$[Fe^{III}_7O_3(OH)_3]^{12+}$	tet Fe^{III}	$^{21}/_2$	30
$[Fe_7O_3(OMe)_3(heen)_3Cl_{4.5}(solv)_2]^{1.5+}$ [c]	$[Fe^{III}_7O_3]^{15+}$	tet Fe^{III}	$^{15}/_2$	31
$[Fe_7O_3(OH)_3Cl(paeo)_6]^{5+}$ [c]	$[Fe^{III}_7O_3(OH)_3]^{12+}$	tet Fe^{III}	$^{21}/_2$	31
$[Fe_7O_3(OMe)_6(O_2CR)_6(MeOH)_6Cl]^{2+}$ [c]	$[Fe^{III}_7O_3]^{15+}$	tet Fe^{III}	$^7/_2$*	32
$[Fe_7O_3(OH)_3(quin)_6]$ [d]	$[Fe^{III}_7O_3(OH)_3]^{12+}$	oct Fe^{III}	$^3/_2$	33
$[Fe_7(OH)_6(quin)_6]^{1+}$ [d]	$[Fe^{III}_7(OH)_6]^{15+}$	oct Fe^{III}	$^3/_2$	33
$[Fe_7(bmsae)_6(OMe)_6]^{2+}$ [d]	$[Fe^{II}Fe^{III}_6]^{20+}$	oct Fe^{II}	n.r.	34
$[Fe_7(tea)_6]^{2+}$ [d]	$[Fe^{II}Fe^{III}_6]^{20+}$	oct Fe^{II}	$^5/_2$*	35
$[Fe_7(L^1)_6\ Cl_6]$ [e]	$[Fe^{II}_3Fe^{III}_4]^{18+}$	oct Fe^{III}	n.r.	36
$[Fe_7(Hbmsae)_6(OMe)_6]^{2+}$ [e]	$[Fe^{II}_7]^{14+}$	oct Fe^{II}	10*	34
$[Fe_7(OMe)_6(HL^2)_6]^{3+}$ [e]	$[Fe^{II}_6Fe^{III}]^{15+}$	oct Fe^{III}	$^{29}/_2$	37
$[Fe_7L^3_6]^{2+}$ [e]	$[Fe^{II}_7]^{14+}$	oct Fe^{II}	n.r.	38

t.w. = this work, n.r. = not reported, oct = octahedral, tet = tetrahedral, * = some uncertainty.

[a] $mdaH_2$ = *N*-methyldiethanolamine; $bdaH_2$ = *N*-butyldiethanolamine; $phdaH_2$ = phenyldiethanolamine; $teaH_3$ = triethanolamine; $bheapH_3$ = 1-[*N*,*N*-bis(2-hydroxyethyl)-amino]-2-propanol; hmpip = 2-hydroxymethylpiperidine; $heenH_2$ = *N*,*N*'-bis(2-hydroxyethyl)ethylenediamine; paeoH = 2-(2-pyridylmethyl)amino-ethanol; $quinH_5$ = D-(-)-quinic acid; H_2bmsae = 5-bromo-3-methoxysalicylideneaminoethanol; H_2L^1 = 2-amino-2-methyl-1,3-propanediol; H_2L^2 = 3-methoxy-2-salicylidenamino-1-ethanol; H_2L^3 = 2-(2-hydroxy-3-methoxybenzylideneamino)phenol; solv = MeOH or H_2O.

[b] central Fe surrounded by a non-planar Fe_6 loop.

[c] non-planar dome or central Fe above a planar Fe_6 loop.

[d] central Fe surrounded by a coplanar Fe_6 loop.

[e] central Fe surrounded by a nearly planar Fe_6 loop.

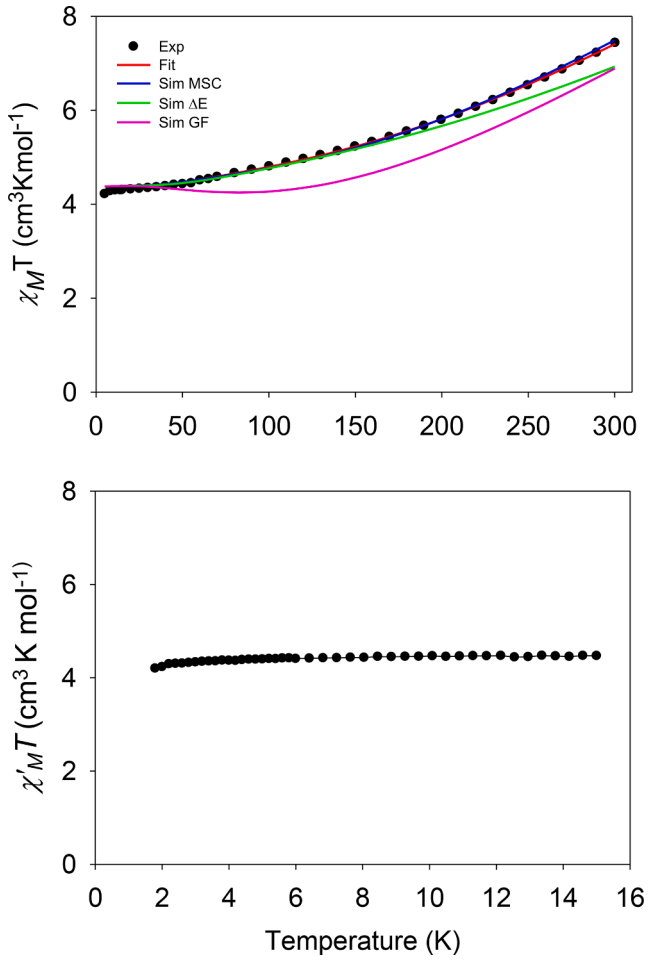

Fig. 2. (**top**) $\chi_M T$ vs T in a 0.1 T dc field, its simulations using the J_{MSC} (—), the $J_{\Delta E}$ (—), and the J_{GF} (—) values, and the J_{PHI} fit (—); (**bottom**) ac in-phase $\chi'_M T$ vs T plot with a 1000 Hz oscillation frequency (Colour online).

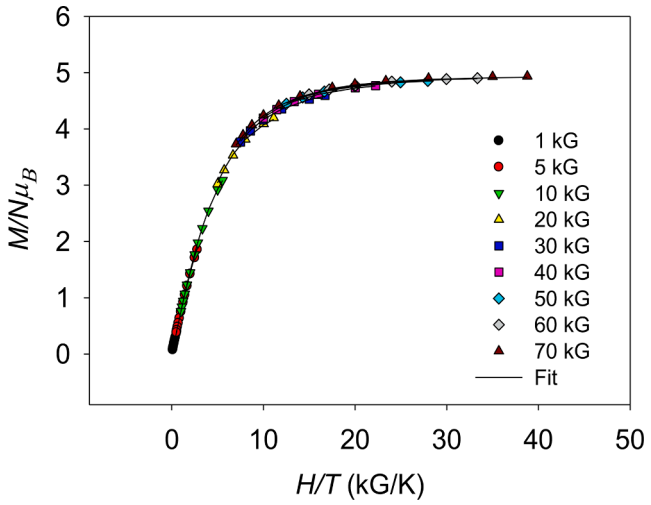

Fig. 3. Plot of reduced magnetization ($M/N\mu_B$) vs H/T data for **1** in the 1.8–10.0 K range at the indicated applied dc fields. The solid lines are the fit of the data; see the text for the fit parameters (Colour online).

produce a convenient initial guess for self-consistent calculations. No symmetry was assumed in the broken-symmetry, GF, or DFT calculations. A self-consistency convergence threshold of 10^{-6} Ha = 0.2 cm^{-1} in the energy and 10^{-8} in the RMS changes in the density matrix was used in all calculations. The GF approach results were calculated using an in-house post-processing code.

3. Results and discussion

3.1. Synthesis

After investigating many reagent ratios, the reaction of $[Fe_3O(O_2C^tBu)_6(H_2O)_3](NO_3)$ with $mdaH_2$ in a 1:~3 ratio in MeCN was found to lead to subsequent isolation of brown X-ray quality crystals of $[Fe_7O_3(O_2C^tBu)_9(mda)_3(H_2O)_3]$ (**1**) in analytical purity from an MeCN/Et_2O layering; the preparation is summarized in Eq. (4).

$$7\ [Fe_3O(O_2CR)_6(H_2O)_3]^+ + 9\ mdaH_2 \rightarrow 3\ [Fe_7O_3(O_2CR)_9(mda)_3(H_2O)_3] + 15\ RCO_2H + 10\ H_2O + 7\ H^+ \quad (4)$$

approximation is given by Eq. (3),

$$J_{GF} = \frac{1}{4S_AS_B}\left[\sum_{i,a}\sum_{\mu,\nu\in A}\sum_{\mu',\nu'\in B}\frac{f_i^\alpha - f_a^\beta}{\epsilon_a^\beta - \epsilon_i^\alpha}C_{\mu i}^\alpha\left(F_{\mu\nu}^\alpha - F_{\mu\nu}^\beta\right)C_{\nu a}^\beta C_{\mu' i}^\alpha\left(F_{\mu'\nu'}^\alpha - F_{\mu'\nu'}^\beta\right)C_{\nu' a}^\beta\right] \quad (3)$$

where F is the local Kohn-Sham (KS) Fock matrix and C is the KS molecular orbital coefficients in a Löwdin orthonormalized basis. The sum runs over the spin center indices μ and ν of site A, μ' and ν' of site B, and i and a are over occupied and virtual orbitals, respectively. For full details of the formulation, we refer the reader to the work of Steenbock [21].

Electronic structure calculations were performed using the Gaussian 16 computation software suite [23]. The Pople all-electron 6-311 + G** basis set is used for Fe and the 6-31G** is used for the ligand atoms. DFT calculations in this work employ the hybrid PBE approximation (PBEh) [24,25] without including relativistic effects. All broken-symmetry DFT energies were obtained using an in-house version of the Gaussian 16 program that allows for a local spin inversion at any magnetic center to

1 can also be obtained by slow evaporation of the filtrate, but with a lower crystal quality.

3.2. Description of structure

Complex **1** crystallizes in the rhombohedral space group $R\bar{3}$ with the Fe_7 cluster lying on a C_3 symmetry axis. The complete structure, labeled core, and a stereopair are shown in Fig. 1, and selected bond distances and angles are listed in Table 2. The core consists of a central Fe^{III} ion (Fe1) held within a non-planar Fe_6 loop (Fe2, Fe3, and their symmetry-equivalent partners) by three μ_3-O^{2-} (O2) ions and three μ_2-EtO^- (O1) arms from the three mda^{2-} groups. All Fe^{III} have near-octahedral geometry, and both the Fe oxidation states and O protonation levels were confirmed by bond valence sum (BVS) calculations [26] (Table 3). Each mda^{2-} group is O,N,O- tridentate chelating on the Fe2 ions, with one alkoxide O1 bridging to the central Fe1, as stated, and the other, O3, bridging to Fe3. As a result, monoatomic bridging of Fe_2 pairs around

Table 5
Exchange interactions J_1 - J_4 for **1** from MSC calculations, DFT computations, and fits of the experimental dc data.

			Calculated J_{ij}			J_{ij} from fits					
J[a]	Fe-O bonds[b]	Fe-O-Fe angles[b]	J_{MSC}	$J_{\Delta E}$ [c]	J_{GF} [c]	J_{PHI} MSC[d]	J_{PHI} ΔE[d]	J_{PHI} GF[d]	J_0 [e]	J_{-10} [e]	J_{-20} [e]
J_1	1.872	119.8	−39.5	−46.3	−41.4	−39.6	−41.0	−34.1	−49.8	−86.4	−37.0
J_2	1.998	127.9	−13.8	−16.2	−14.8	−15.1	−11.4	−16.1	+54.4	−42.9	−14.7
J_3	1.982	97.0	−6.7	−3.9	−13.2	−6.3	−5.0	−9.0	−115.0	+3.4	−7.1
J_4	1.942	134.8	−23.5	−28.1	−24.7	−24.3	−27.3	−36.0	+72.9	+63.0	−29.7

[a]cm^{-1}; $\hat{H} = -2J_{ij}\hat{S}_i \bullet \hat{S}_j$ convention. See labeling in Fig. 4.
[b]Average in Å and deg.
[c]The DFT calculations gave all J_{ij} values independently, so only one is shown for symmetrically equivalent sets. For J_1 and J_3, all three were identical. For J_2 and J_4, one value differed by 0.1 cm^{-1}.
[d]Fits of experimental data using the indicated J_{ij} as inputs; a constant TIP = 700 ×!0^{-6} cm^3/mol was also included.
[e]The $J_{\#}$ are the fit values obtained using the given # as J_1 - J_4 input values.

the outer Fe_6 loop alternates between an mda^{2-} μ_2-EtO$^-$ (O3) and a μ_3-O^{2-} (O2). Each of the latter Fe2Fe3 pairs is also bridged by two syn,syn η^1:η^1:μ-^{t}BuCO$_2^-$ ligands, and peripheral ligation is completed by a monodentate ^{t}BuCO$_2^-$ group and a terminal water molecule (O8) on each Fe3, and these form intramolecular hydrogen-bonds between them involving the unbound carboxylate O9 atom (O8···O9 = 2.574(8) Å). There are also hydrogen-bonds between the terminal O8 water ligands (O8···O8 = 2.986(8) Å) [Fig. S1]. Complex **1** joins a family of eighteen Fe_7 complexes with the general description of a central Fe surrounded by an Fe_6 array (Table 4) [27–38]. Only five of these, however, have the same structural topology as **1**, i.e., a $[Fe^{III}_7O_3]^{15+}$ core with a central octahedral Fe^{III} ion surrounded by a non-planar Fe_6 loop [27–29].

3.3. SQUID magnetometry

3.3.1. Magnetic susceptibility studies

Solid-state, variable-temperature dc magnetic susceptibility (χ_M) data for **1** in the 5.0–300 K range were collected on crushed vacuum-dried microcrystalline samples restrained in eicosane to prevent torquing. $\chi_M T$ decreases steadily from 7.4 cm^3 K mol^{-1} at 300 K to 4.2 cm^3 K mol^{-1} at 5.0 K [Fig. 2]. The 300 K value is much lower than the 30.6 cm^3 K mol^{-1} calculated for seven non-interacting high-spin Fe^{III} ions ($S = {}^5/_2$) with $g = 2.00$, indicating dominant antiferromagnetic (**AF**) interactions. The near-constant value at 5.0 K suggests an $S = {}^5/_2$ ground state and was supported by ac magnetic susceptibility measurements performed in the 1.8 to 15 K range in a 3.5 G ac field at a 1000 Hz oscillation frequency. The ac in-phase $\chi'_M T$ vs T and out-of-phase χ''_M vs T plots are shown in Fig. 2 and Fig. S2, respectively. $\chi'_M T$ is near-constant at ~ 4.3 cm^3 K mol^{-1} in the 1.8–15 K range, confirming a well-isolated $S = {}^5/_2$ ground state. There was no χ''_M signal.

Further confirmation for a $S = {}^5/_2$ ground state was obtained from magnetization (M) vs field (H) and T data collected in the 0.1–7.0 T and 1.8–10.0 K ranges and plotted as $M/N\mu_B$ vs H/T in Fig. 3, where N is Avogadro's number and μ_B is the Bohr magneton. The data were fit by diagonalization of the spin Hamiltonian matrix using program MAGNET [14], which assumes that only the ground state is occupied, includes axial zero-field splitting (zfs), $D\hat{S}_z^2$, and the Zeeman interaction, and incorporates a full powder average. The corresponding spin Hamiltonian is given by Eq. (5), where μ_B is the Bohr magneton, D is the axial zfs parameter, and μ_0 is the vacuum permeability. An excellent fit

$$H = D\hat{S}_z^2 + g\mu_B\mu_0\hat{S}\cdot H \quad (5)$$

(solid lines in Fig. 3) was obtained with $S = {}^5/_2$, $D = -0.42$ cm^{-1} and $g = 1.98$. A second fit with a positive D also gave an excellent fit to the data, as expected, with $S = {}^5/_2$, $D = +0.51$ cm^{-1}, and $g = 1.99$. The D vs g error surface generated using the program GRID [15] (Fig. S3) revealed both fits to be of essentially equal quality, with a slightly greater softness in the positive D. The fit values obtained in the present work are reasonably comparable with those obtained by our previous EPR study of **1**, in which simulations of the EPR spectra indicated an $S = {}^5/_2$ ground state with $g = 2.00(1)$ and $D = +0.36$ cm^{-1} [10].

3.3.2. Ground state spin rationalization using MSC and DFT methods

An important objective in molecular magnetism is to achieve insight into how the spin vectors at the various paramagnetic metal ions in a polynuclear cluster are aligned in the ground state and thus lead to the experimentally observed ground state spin. Such a rationalization of an experimental conclusion requires determination of the pairwise exchange couplings (J_{ij}) between the metal ions, which would then allow the strongest couplings to be identified, as well the presence of any spin frustration effects. To achieve this for **1**, we implemented a three-pronged analysis consisting of (i) a semiempirical MSC for polynuclear Fe^{III}/O clusters [9] to obtain J_{MSC}, (ii) DFT computations using both standard broken symmetry energy differences to obtain $J_{\Delta E}$ and the Green's function approximation method to get J_{GF}, and (iii) fits of experimental $\chi_M T$ vs T data using the program PHI [11] to obtain J_{PHI}. We first carried out approaches (i) and (ii) to compare the obtained J_{MSC}, $J_{\Delta E}$, and J_{GF}, followed by then using them as credible input values in fits of the experimental data; we have found in previous work that this approach minimizes problems with overparameterization and thus resulting 'false' fits not related to the real J_{ij} of the cluster. The calculated J_{MSC}, $J_{\Delta E}$, J_{GF}, and J_{PHI} for **1** are listed in Table 5.

In accord with the protocol set forth for the Mitchell-Christou polynuclear Fe^{III}/O MSC [9], the Fe-O bond lengths (r) and Fe-O-Fe angles (φ) for each Fe_2 pair were used with Eq. (6) to generate the J_{MSC} for **1**. In instances of multiple monoatomic oxo bridges between two Fe^{III} ions, the longer average Fe^{III}-O bond was used, as per the protocol [9].

$$J_{ij} = (1.23 \times 10^9)(-0.12 + 1.57\cos\varphi + \cos^2\varphi)e^{-8.99r} \quad (6)$$

The crystallographic C_3 symmetry of **1** gives rise to four independent J_{ij} parameters: J_1 and J_2 in the outer Fe_6 loop, and J_3 and J_4 to the central Fe1 (Fig. 4). The J_1 - J_4 determined from the M−C MSC and the two types of theoretical calculations are in agreement in both sign and magnitude (Table 5), with the biggest discrepancy being in the magnitude of J_3 between the J_{MSC} (−6.7 cm^{-1}) and $J_{\Delta E}$ (−3.9 cm^{-1}) values and the J_{GF} (−13.2 cm^{-1}) value. Note that the DFT calculations are on the complete heptanuclear complex, and are thus affected by the total metal nuclearity, whereas the MSC calculations are performed on one Fe_2 pair at a time and are not affected by the metal nuclearity. The resulting agreement between the different approaches is thus very satisfying and reflects the power of modern computational methods.

All J_1 - J_4 interactions are **AF**, which is almost always the case for high spin Fe^{III} systems, with the weakest interaction being J_3 in the Fe_2 pairs with two monoatomic oxo bridges giving small Fe-O-Fe angles (97.0° and 99.0°); the stronger J_1, J_2, and J_4 all involve single monoatomic oxo bridges and consequently larger Fe-O-Fe angles (119.8–134.8°). Since all interactions are **AF** and the Fe_7 topology comprises six edge-fused Fe_3 triangles, the complex is expected to experience spin frustration, here defined in the way most appropriate for molecular systems as competing exchange interactions that prevent

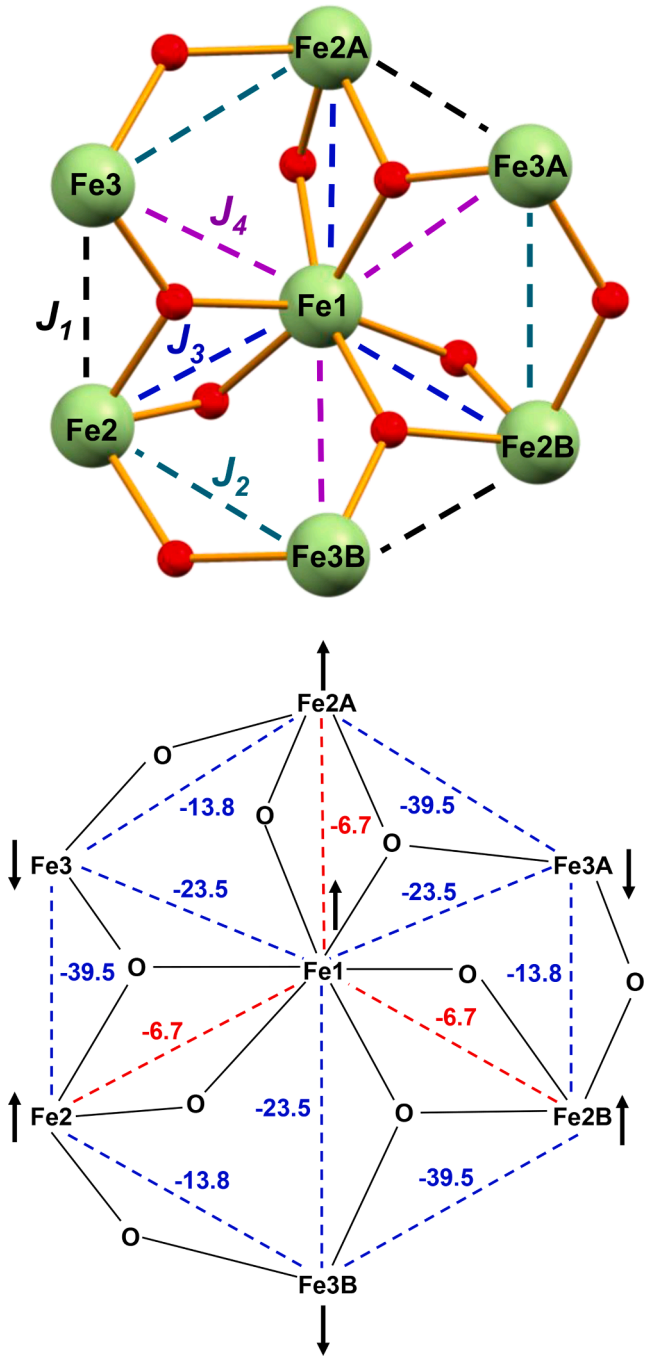

Fig. 4. (**top**) Fe^{III}/O/OR core of **1** showing the J_1 - J_4 exchange-coupling scheme for the J_{MSC}, $J_{\Delta E}$, and J_{GF} calculations. Color code: Fe^{III} lime green, O red. (**bottom**) Diagrammatic representation of the Fe atoms in **1** showing the J_{MSC} exchange-couplings (cm^{-1}), the spin frustrated pathways, and the relative spin alignments determined from them. The latter are the same when the $J_{\Delta E}$ or J_{GF} values are employed. Color code: satisfied pathways are blue, frustrated pathways are red. The $m_s = \pm^5/_2$ *z*-components of spin are shown as up and down black arrows. ((Colour online.))

(frustrate) the preferred spin vector alignments. J_1 and J_4 are both strong relative to J_2 and J_3, which are intermediate and weak, respectively, so the former two dominate leading to antiparallel alignments both between Fe1 and the Fe3/Fe3A/Fe3B set, and between the latter and the Fe2/Fe2A/Fe2B set. This gives an alternating 'spin-up, spin-down' alignment pattern around the outer Fe_6 loop corresponding to $m_s = \pm^5/_2$ *z*-components of spin, and 'spin-up' on the central Fe1 (Fig. 4). This situation also satisfies the J_2 interactions, but the resulting parallel alignments between Fe1 and the Fe2/Fe2A/Fe2B set frustrate J_3 (red dashed lines in Fig. 4, bottom), which is **AF** but much too weak to compete with J_1 and J_4. This is the reason that an Ising-like 'spin-up'/'spin-down' alignment corresponding to $m_s = \pm^5/_2$ *z*-components of spin results, rather than any intermediate spin vector alignments. Thus, the total spin of **1** is $S = {}^{20}/_2 - {}^{15}/_2 = {}^5/_2$, rationalizing the experimentally observed ground state. Note that the same spin vector alignments and overall $S = {}^5/_2$ are obtained when either the J_{MSC}, $J_{\Delta E}$, or J_{GF} values for J_1-J_4 are used in this analysis (Fig. S4).

The J_{MSC} and $J_{\Delta E}$ both give good simulations using program PHI [11] of the experimental $\chi_M T$ vs T data (blue and green lines, respectively, in Fig. 2), but the simulation with J_{GF} was poorer. We then used all the calculated values in turn as inputs for fits of the experimental data and all gave excellent fits with the fit parameters in Table 5; the fit using J_{MSC} is shown in as the solid red line in Fig. 2). The three sets of fit parameters are all satisfyingly comparable, with those from the J_{MSC} and $J_{\Delta E}$ inputs being particularly similar to each other and to the input values they came from. Those from J_{GF} inputs show greater variation from the J_{MSC} and $J_{\Delta E}$ fit values, but we note that J_3 is now a more reasonable − 9.0 cm^{-1}. Its stronger −13.2 cm^{-1} in the calculated J_{GF}, making it comparable with J_2 (−14.8 cm^{-1}), is probably the main reason the simulation using J_{GF} values was poor, since the J_3 would not be completely frustrated in this case. Notwithstanding such small discrepancies between the values, the overall picture that emerges is that the three methods – DFT computations, MSC calculations, and experimental fits – give excellent agreement in the relative magnitude of the J_{ij} as strong (J_1, J_4), intermediate (J_2), and weak (J_3), and thereby rationalizing the experimental ground state of **1** by identifying the resulting spin vector alignments. To support our statement that the J_{MSC}, $J_{\Delta E}$ and J_{GF} are similar, we include in Table 5 the result of control fits of the experimental data using J_1 - J_4 input values of 0, −10, and −20 cm^{-1}. The resulting J_0, J_{-10}, and J_{-20} are extremely different to each other and to the J_{MSC}, $J_{\Delta E}$ and J_{GF}; the large **F** couplings are particular unrealistic for high-spin Fe^{III}. This supports the benefits of the synergistic use of MSC and DFT as both an internal check on each other and as a route to reliable approximations of J_{ij} values as inputs for fits of experimental data that will lead to believable J_{ij} fit values.

4. Conclusions

We are finally able to provide a publishable crystal structure of complex **1** to complement the previously published EPR spectral data [10], and we have also taken the opportunity to carry out a three-pronged study of its magnetic properties. The C_3 symmetry of the Fe_7 topology comprising a central octahedral Fe^{III} within a non-planar Fe_6 loop results in this being a 4-*J* system. The application of the three-pronged analysis has provided a synergistic means to minimize over-parameterization problems in fitting of experimental magnetism data by providing credible J_{ij} values to use as inputs. These have also allowed identification of spin frustration effects in **1**, and thus identification of spin vector alignments that lead to the experimentally-determined $S = {}^5/_2$ ground state. The power of DFT methods coupled with the simplicity of the MSC has proven beneficial and supports the utility of this approach in the analysis of the magnetic properties of other Fe^{III}/O clusters of various metal nuclearities. Such studies are in progress.

Declaration of Competing Interest

The authors declare that they have no known competing financial interests or personal relationships that could have appeared to influence the work reported in this paper.

Data availability

Data will be made available on request.

Acknowledgments

This work was supported by the U.S. National Science Foundation (Grant CHE-1900321), and by the Department of Energy, Office of Science, Office of Basic Energy Sciences, as part of the Computational Chemical Sciences Program under Award #DE-SC0018331. LEA is supported by the Office of Basic Energy Sciences, US Department of Energy, grant DE-SC0005027. We thank the NSF for funding of the X-ray diffractometer through grant CHE-1828064.

Appendix A. Supplementary data

Supplementary data to this article can be found online at https://doi.org/10.1016/j.poly.2022.116045.

References

[1] (a) S. Ménage, V. Zang, M. P. Hendrich, L. Que, Diferrous Core of Ribonucleotide Reductase, J. Am. Chem. Soc. 2 (7) 1992 7786–7792, https://doi.org/10.1021/ja00046a026. (b) S. Herold, S.J. Lippard, Carboxylate-bridged diiron(II) complexes: Synthesis characterization, and O2-reactivity of models for the reduced diiron centers in methane monooxygenase and ribonucleotide reductase, J. Am. Chem. Soc. 119 (1997) 145–156, https://doi.org/10.1021/ja9628563.

[2] D. Lee, S.J. Lippard, Structural and functional models of the dioxygen-activating centers of non-heme diiron enzymes ribonucleotide reductase and soluble methane monooxygenase, J. Am. Chem. Soc. 120 (1998) 12153–12154, https://doi.org/10.1021/ja9831094.

[3] (a) H. Toftlund, K.S. Murray, P.R. Zwack, L.F. Taylor, O.P. Anderson, Structural and electronic properties of tetranuclear iron(III) pyridylamine complexes containing cofacial pairs of μ-oxo-bis(μ-acetato)iron(III) moieties. Models for met hemerythrins, J. Chem. Soc. Chem. Commun. (1986) 191–193, https://doi.org/10.1039/C39860000191. (b) B. Mauerer, J. Crane, J. Schuler, K. Wieghardt, B. Nuber, A Hemerythrin Model Complex with Catalase Activity, Angew. Chemie Int. Ed. English. 32 (1993) 289–291, https://doi.org/10.1002/anie.199302891. (c) H. Arii, S. Nagatomo, T. Kitagawa, T. Miwa, K. Jitsukawa, H. Einaga, H. Masuda, A novel diiron complex as a functional model for hemerythrin, J. Inorg. Biochem. 82 (2000) 153–162, https://doi.org/10.1016/S0162-0134(00)00163-X.

[4] (a) S. Herold, S.J. Lippard, Carboxylate-bridged diiron(II) complexes: Synthesis characterization, and O_2-reactivity of models for the reduced diiron centers in methane monooxygenase and ribonucleotide reductase, J. Am. Chem. Soc. 119 (1997) 145–156, https://doi.org/10.1021/ja9628563. (b) D. Coucouvanis, R.A. Reynolds, W.R. Dunham, Synthesis and Characterization of a New Class of Asymmetric Aqua—Acetate Bridged Dimers. Solid State Molecular Structures of the $[M(\mu\text{-}H_2O)(\mu\text{-}OAc)_2(OAc)_3(Py)_2^-$ Anions (M = Mn (II), Fe (II), Co (II)). A Structural Model for the Fe_2 Site in Methane Monooxygenase, J. Am. Chem. Soc. 117 (1995) 7570–7571, https://doi.org/10.1021/ja00133a041. (c) K. Kim, S.J. Lippard, Structure and Mossbauer spectrum of a (μ-1,2-peroxo)bis(μ-carboxylato)diiron(III) model for the peroxo intermediate in the methane monooxygenase hydroxylase reaction cycle, J. Am. Chem. Soc. 118 (1996) 4914–4915, https://doi.org/10.1021/ja9604370. (d) M. Sankaralingam, M. Palaniandavar, Diiron(III) complexes of tridentate 3N ligands as functional models for methane monooxygenases: Effect of the capping ligand on hydroxylation of alkanes, Polyhedron. 67 (2014) 171–180, https://doi.org/10.1016/j.poly.2013.08.067.

[5] S.J. Lippard, Oxo-Bridged Polyiron Centers in Biology and Chemistry, Angew. Chemie Int. Ed. English 27 (1988) 344–361, https://doi.org/10.1002/anie.198803441.

[6] (a) E.C. Theil, Ferritin: structure, gene regulation, and cellular function in animals, plants, and microorganisms., Annu. Rev. Biochem. 56 (1987) 289–315, https://doi.org/10.1146/annurev.bi.56.070187.001445. (b) E.C. Theil, M. Matzapetakis, X. Liu, Ferritins: Iron/oxygen biominerals in protein nanocages, J. Biol. Inorg. Chem. 11 (2006) 803–810, https://doi.org/10.1007/s00775-006-0125-6. (c) A. Bino, M. Ardon, D. Lee, B. Spingler, S.J. Lippard, Synthesis and structure of [Fe13O4F24(OMe)125-: The first open-shell Keggin ion, J. Am. Chem. Soc. 124 (2002) 4578–4579, https://doi.org/10.1021/ja025590a.

[7] (a) C. Cañada-Vilalta, T.A. O'Brien, E.K. Brechin, M. Pink, E.R. Davidson, G. Christou, Large spin differences in structurally related Fe6 molecular clusters and their magnetostructural explanation, Inorg. Chem. 43 (2004) 5505–5521, https://doi.org/10.1021/ic049413h. (b) J.K. McCusker, E.A. Schmiit, P.M. Hagen, D.N. Hendrickson, J.B. Vincent, M.L. Mino, K. Shin, D.A.K. Coggin, G. Christou, J.C. Huffman, Molecular Spin Frustration in the [Fe4O28+ Core: Synthesis, Structure, and Magnetochemistry of [Fe4O2(O2CR)7(bpy)2(ClO4) (R = Me, Ph), J. Am. Chem. Soc. 113 (1991) 3012–3021. https://doi.org/10.1021/ja00008a033. (c) A. P. Singh, R.P. Joshi, K.A. Abboud, J.E. Peralta, G. Christou, Molecular spin frustration in mixed-chelate Fe5 and Fe6 oxo clusters with high ground state spin values, Polyhedron. 176 (2020), https://doi.org/10.1016/j.poly.2019.114182.

[8] (a) K. Weighardt, K. Pohl, I. Jibril, G. Huttner, Hydrolysis Products of the Monomeric Amine Complex $(C_6H_{15}N_3)FeCl_3$: The Structure of the Octameric Iron (III) Cation of $\{[C_6H_{15}N_3)_6Fe_8(\mu_3\text{-}O)_2(\mu_2\text{-}OH)_{12}Br_7(H_2O)\}Br\cdot 8H_2O$. Angew. Chem. Int. Ed. 21 (1) 1984 77-78, https://doi.org/10.1002/anie.198400771 (b) A.L. Barra, P. Debrunner, D. Gatteschi, C.E. Schulz, R. Sessoli, Superparamagnetic-like behavior in an octanuclear iron cluster, Europhys. Lett. 35 (1996) 133–138, https://doi.org/10.1209/epl/i1996-00544-3. (c) A.L. Barra, A. Caneschi, A. Cornia, F. De Fabrizi Biani, D. Gatteschi, C. Sangregorio, R. Sessoli, L. Sorace, Single-molecule magnet behavior of a tetranuclear iron(III) complex. The origin of slow magnetic relaxation in iron(III) clusters, J. Am. Chem. Soc. 121 (1999) 5302–5310, https://doi.org/10.1021/ja9818755. (d) A.K. Boudalis, B. Donnadieu, V. Nastopoulos, J.M. Clemente-Juan, A. Mari, Y. Sanakis, J.P. Tuchagues, S.P. Perlepes, A nonanuclear iron(II) single-molecule magnet, Angew. Chem., Int. Ed. 43 (2004) 2266–2270, https://doi.org/10.1002/anie.200353147. (e) S. Accorsi, A. L. Barra, A. Caneschi, G. Chastanet, A. Cornia, A.C. Fabretti, D. Gatteschi, C. Mortalò, E. Olivieri, F. Parenti, P. Rosa, R. Sessoli, L. Sorace, W. Wernsdorfer, L. Zobbi, Tuning anisotropy barriers in a family of tetrairon(III) single-molecule magnets with an $S = 5$ ground state, J. Am. Chem. Soc. 128 (2006) 4742–4755, https://doi.org/10.1021/ja0576381. (f) C. Schlegel, E. Burzurí, F. Luis, F. Moro, M. Manoli, E.K. Brechin, M. Murrie, J. Von Slageren, Magnetic properties of two new Fe_4 single-molecule magnets in the solid state and in frozen solution, Chem. - A Eur. J. 16 (2010) 10178–10185. https://doi.org/10.1002/chem.200903505. (g) Y. Y. Zhu, T.T. Yin, S. Da Jiang, A.L. Barra, W. Wernsdorfer, P. Neugebauer, R. Marx, M. Dörfel, B.W. Wang, Z.Q. Wu, J. van Slageren, S. Gao, The solvent effect in an axially symmetric Fe_4^{III} single-molecule magnet, Chem. Commun. 50 (2014) 15090–15093. https://doi.org/10.1039/c4cc07580c. (h) Y.Y. Zhu, C. Cui, K. Qian, J. Yin, B.W. Wang, Z.M. Wang, S. Gao, A family of enantiopure Fe_4^{III} single molecule magnets: Fine tuning of energy barrier by remote substituent, Dalt. Trans. 43 (2014) 11897–11907, https://doi.org/10.1039/c3dt53317d. (i) L. Rigamonti, M. Piccioli, A. Nava, L. Malavolti, B. Cortigiani, R. Sessoli, A. Cornia, Structure, magnetic properties and thermal sublimation of fluorinated Fe_4 Single-Molecule Magnets, Polyhedron. 128 (2017) 9–17, https://doi.org/10.1016/j.poly.2017.02.036. (j) S. Liu, Y.F. Deng, C. Li, X. Chang, Y.Z. Zhang, A linear trinuclear ferrous single molecule magnet, Dalt. Trans. 47 (2018) 16704–16708, https://doi.org/10.1039/c8dt03410a. (k) S.K. Barman, J. Cano, F. Lloret, R. Mukherjee, Single-Molecule-Magnet $Fe_4^{II}Fe_2^{III}$ and Antiferromagnetic Fe_4^{III} Coordination Clusters, Inorg. Chem. 58 (2019) 8086–8099, https://doi.org/10.1021/acs.inorgchem.9b00828. (l) C. Benelli, J. Cano, Y. Journaux, R. Sessoli, G. A. Solan, R.E.P. Winpenny, A decanuclear iron(III) single molecule magnet: Use of Monte Carlo methodology to model the magnetic properties, Inorg. Chem. 40 (2001) 188–189, https://doi.org/10.1021/ic000840e. (m) J.C. Goodwill, R. Sessoli, D. Gatteschi, W. Wernsdorfer, A.K. Powell, S.L. Heath, Towards nanostructured arrays of single molecule magnets: New Fe_{19} oxyhydroxide clusters displaying high ground state spins and hysteresis, J. Chem. Soc. Dalton Trans. (2000) 1835–1840. https://doi.org/10.1039/b002135k.

[9] K.J. Mitchell, K.A. Abboud, G. Christou, Magnetostructural Correlation for High-Nuclearity Iron(III)/Oxo Complexes and Application to Fe_5, Fe_6, and Fe_8 Clusters, Inorg. Chem. 55 (2016) 6597–6608, https://doi.org/10.1021/acs.inorgchem.6b00769.

[10] S. Datta, A. Betancur-Rodriguez, S.C. Lee, S. Hill, D. Foguet-Albiol, R. Bagai, G. Christou, EPR characterization of half-integer-spin iron molecule-based magnets, Polyhedron 26 (2007) 2243–2246, https://doi.org/10.1016/j.poly.2006.11.006.

[11] N.F. Chilton, R.P. Anderson, L.D. Turner, A. Soncini, K.S. Murray, PHI: A powerful new program for the analysis of anisotropic monomeric and exchange-coupled polynuclear *d*- and *f*-block complexes, J. Comput. Chem. 34 (2013) 1164, https://doi.org/10.1002/jcc.23234.

[12] A.M. Bond, R.J.H. Clark, D.G. Humphrey, P. Panayiotopoulos, B.W. Skelton, A.H. White, Synthesis, characterisation and electrochemical reductions of oxo-centred, carboxylate-bridged triiron complexes, $[Fe_3(\mu_3\text{-}O)(\mu\text{-}O_2CR)_6L_3X$ (R = Me, Bu^t, Ph, CH_2Cl, CCl_3, CH_2CN or 4-$NO_2C_6H_4$; L = py, 3-H_2Npy, 4-H_2Npy, 3-NCpy, 4-NCpy or 4-CH_2CHpy; X = ClO_4^- or NO_3^-), J. Chem. Soc., Dalton Trans. 11 (1998) 1845–1852, https://doi.org/10.1039/A708880I.

[13] G.M. Sheldrick, Crystal structure refinement with *SHELXL*, Acta Cryst. C 71 (2015) 3–8, https://doi.org/10.1107/S2053229614024218.

[14] E.R. Davidson, MAGNET, Indiana University, Bloomington, IN, 1999.

[15] E.R. Davidson GRID, Indiana University 1999 Bloomington IN.

[16] G.A. Bain, J.F. Berry, Diamagnetic Corrections and Pascal's Constants, J. Chem. Educ. 85 (2008) 532, https://doi.org/10.1021/ed085p532.

[17] L. Noodleman, Valence bond description of antiferromagnetic coupling in transition metal dimers, J. Chem. Phys. 74 (1981) 5737–5743, https://doi.org/10.1063/1.440939.

[18] (a) C. Van Wüllen, Broken symmetry approach to density functional calculation of magnetic anisotropy or zero field splittings for multinuclear complexes with antiferromagnetic coupling, J. Phys. Chem. A. 113 (2009) 11535–11540, .; (b) A. Bencini, F. Totti, C.A. Daul, K. Doclo, P. Fantucci, V. Barone, Density Functional Calculations of Magnetic Exchange Interactions in Polynuclear Transition Metal Complexes, Inorg. Chem. 36 (1997) 5022–5030, .; (c) E. Ruiz, A. Rodríguez-Fortea, J. Cano, S. Alvarez, P. Alemany, About the calculation of exchange coupling constants in polynuclear transition metal complexes, J. Comput. Chem. 24 (2003) 982–989, .; (d) R. Valero, R. Costa, I. De P. R. Moreira, D.G. Truhlar, F. Illas, Performance of the M06 family of exchange-correlation functionals for predicting magnetic coupling in organic and inorganic molecules, J. Chem. Phys. 128 (2008), .; (e) P. Comba, S. Hausberg, B. Martin, Calculation of exchange coupling constants of transition metal complexes with DFT, J. Phys. Chem. A. 113 (2009) 6751–6755, .

[19] A.I. Liechtenstein, M.I. Katsnelson, V.P. Antropov, V.A. Gubanov, Local Spin Density Functional Approach to the Theory of Exchange Interactions In Ferromagnetic Metals and Alloys, J. Magn. Magn. Mater. 67 (1987) 65–74, https://doi.org/10.1016/0304-8853(87)90721-9.

[20] M.J. Han, T. Ozaki, J. Yu, Electronic structure, magnetic interactions, and the role of ligands in M_n (n = 4,12) single-molecule magnets, Phys. Rev. B 70 (2004) 1–10, https://doi.org/10.1103/PhysRevB.70.184421.

[21] T. Steenbock, J. Tasche, A.I. Lichtenstein, C. Herrmann, A Green's-Function Approach to Exchange Spin Coupling As a New Tool for Quantum Chemistry, J. Chem. Theory Comput. 11 (2015) 5651–5664, https://doi.org/10.1021/acs.jctc.5b00349.

[22] L. E. Aebersold, A. R. Hale, G. Christou, and J. E. Peralta. A thorough validation of the Green's-function approximation for the calculation of magnetic exchange couplings, manuscript in preparation.

[23] Gaussian 16, Revision C.01, M. J. Frisch, G. W. Trucks, H. B. Schlegel, G. E. Scuseria, M. A. Robb, J. R. Cheeseman, G. Scalmani, V. Barone, G. A. Petersson, H. Nakatsuji, X. Li, M. Caricato, A. V. Marenich, J. Bloino, B. G. Janesko, R. Gomperts, B. Mennucci, H. P. Hratchian, J. V. Ortiz, A. F. Izmaylov, J. L. Sonnenberg, D. Williams-Young, F. Ding, F. Lipparini, F. Egidi, J. Goings, B. Peng, A. Petrone, T. Henderson, D. Ranasinghe, V. G. Zakrzewski, J. Gao, N. Rega, G. Zheng, W. Liang, M. Hada, M. Ehara, K. Toyota, R. Fukuda, J. Hasegawa, M. Ishida, T. Nakajima, Y. Honda, O. Kitao, H. Nakai, T. Vreven, K. Throssell, J. A. Montgomery, Jr., J. E. Peralta, F. Ogliaro, M. J. Bearpark, J. J. Heyd, E. N. Brothers, K. N. Kudin, V. N. Staroverov, T. A. Keith, R. Kobayashi, J. Normand, K. Raghavachari, A. P. Rendell, J. C. Burant, S. S. Iyengar, J. Tomasi, M. Cossi, J. M. Millam, M. Klene, C. Adamo, R. Cammi, J. W. Ochterski, R. L. Martin, K. Morokuma, O. Farkas, J. B. Foresman, and D. J. Fox, Gaussian, Inc., Wallingford CT, 2016.

[24] M. Ernzerhof, G.E. Scuseria, Assessment of the Perdew – Burke – Ernzerhof, J. Chem. Phys. 110 (1999) 5029, https://doi.org/10.1063/1.478401.

[25] C. Adamo, V. Barone, Toward reliable density functional methods without adjustable parameters: The PBE0 model, J. Chem. Phys. 110 (1999) 6158–6170, https://doi.org/10.1063/1.478522.

[26] (a) N. E. Brese, M. O'Keeffe, Bond-valence parameters for solids, Acta Crystallogr. Sect. B Struct. Sci. B47 (1991) 192–197, . (b) W. Liu, H. H Thorp, Bond valence sum analysis of metal-ligand bond lengths in metalloenzymes and model complexes. 2. Refined distances and other enzymes, Inorg. Chem. 32 (1993) 4102–4105, .

[27] A. R. Hale, M. E. Lott, J. E. Peralta, D. Foguet-Albiol, K. A. Abboud, and G. Christou. Magnetic Properties of high nuclearity Fe_x-oxo (x = 7, 22, 24) clusters analyzed by a multi-pronged experimental, computational, and magnetostructural correlation approach, submitted for publication.

[28] A.M. Ako, O. Waldmann, V. Mereacre, F. Klöwer, I.J. Hewitt, C.E. Anson, H. U. Güdel, A.K. Powell, Odd-numbered Fe^{III} complexes: Synthesis, molecular structure, reactivity, and magnetic properties, Inorg. Chem. 46 (2007) 756–766, https://doi.org/10.1021/ic061650s.

[29] L.F. Jones, P. Jensen, B. Moubaraki, K.J. Berry, J.F. Boas, J.R. Pilbrow, K. S. Murray, Heptanuclear iron(iii) triethanolamine clusters exhibiting 'millennium dome'-like topologies and an octanuclear analogue with ground spin states of S = $^5/_2$ and 0, respectively, J. Mater. Chem. 16 (2006) 2690–2697, https://doi.org/10.1039/b602858f.

[30] C.M. Kizas, C. Papatriantafyllopoulou, M. Pissas, Y. Sanakis, A. Javed, A. J. Tasiopoulos, C. Lampropoulos, Synthesis, magnetic and spectroscopic characterization of a new Fe_7 cluster with a six-pointed star topology, Polyhedron 64 (2013) 280–288, https://doi.org/10.1016/j.poly.2013.05.015.

[31] S. Mukherjee, R. Bagai, K.A. Abboud, G. Christou, Raising the spin of Fe_7^{III} disklike clusters: The power of molecular spin frustration, Inorg. Chem. 50 (2011) 3849–3851, https://doi.org/10.1021/ic200256j.

[32] K.C. Mondal, V. Mereacre, G.E. Kostakis, Y. Lan, C.E. Anson, I. Prisecaru, O. Waldmann, A.K. Powell, A Strongly Spin-Frustrated Fe_7^{III} Complex with a Canted Intermediate Spin Ground State of S=$^7/_2$ or $^9/_2$, Chem. Eur. J. 21 (2015) 10835–10842, https://doi.org/10.1002/chem.201500841.

[33] M. Menelaou, E. Vournari, V. Psycharis, C.P. Raptopoulou, A. Terzis, V. Tangoulis, Y. Sanakis, C. Mateescu, A. Salifoglou, Heptanuclear Antiferromagnetic Fe(III) −D–(-)-Quinato Assemblies with an S = 3/2 Ground State-pH-Specific Synthetic Chemistry, Spectroscopic, Structural, and Magnetic Susceptibility Studies, Inorg. Chem. 52 (2013) 13849–13860, https://doi.org/10.1021/ic401036e.

[34] N. Hoshino, A.M. Ako, A.K. Powell, H. Oshio, Molecular magnets containing wheel motifs, Inorg. Chem. 48 (2009) 3396–3407, https://doi.org/10.1021/ic801776w.

[35] T. Liu, B.W. Wang, Y.H. Chen, Z.M. Wang, S. Gao, Syntheses, structures and magnetic properties of two mixed-valent disc-like hepta-nuclear compounds of $[Fe^{II}Fe^{III}_6(tea)_6(ClO_4)_2$ and $[Mn^{II}_3Mn^{III}_4(nmdea)_6(N_3)_6{\cdot}CH_3OH$ (tea = $N(CH_2CH_2O)^{3-}_3$, nmdea = $CH_3N(CH_2CH_2O)^{2-}_2$), Z. Anorg. Allg. Chem. 634 (2008) 778–783, https://doi.org/10.1002/zaac.200700505.

[36] T. Liu, B.W. Wang, Y.H. Chen, Z.M. Wang, S. Gao, Syntheses, structures and magnetic properties of two mixed-valent disc-like hepta-nuclear compounds of $[Fe^{II}Fe^{III}_6(tea)_6](ClO_4)_2$ and $[Mn^{II}_3Mn^{III}_4(nmdea)_6(N_3)_6]{\cdot}CH_3OH$ (tea = N $(CH_2CH_2O)^{3-}_3$, nmdea = $CH_3N(CH_2CH_2O)^{2-}_2$), Z. Anorg. Allg. Chem. 634 (2008) 778–783, .

[37] H. Oshio, N. Hoshino, T. Ito, M. Nakano, F. Renz, P. Gütlich, High-spin wheel of a heptanuclear mixed-valent $Fe^{II,\ II}I$ complex, Angew. Chem. Int. Ed. 42 (2003) 223–225, https://doi.org/10.1002/anie.200390084.

[38] H. Zhang, J. Zhang, R. Liu, Y. Li, W. Liu, W. Li, Five Disk-Shaped MII7 (M = Mn, Fe Co, Cu, Zn) Clusters and One Capsule-Like CuII6NaI2 Cluster Assembled from the Same Schiff Base Ligand, Eur. J. Inorg. Chem. 26 (2016) 4134–4143, https://doi.org/10.1002/ejic.201600455.